J. Water Environ. Nanotechnol., 7(1): 69-88 Winter 2022

ORIGINAL RESEARCH PAPER

Magnetic pectin nanocomposite for efficient adsorption of heavy metals from aqueous solution

Sadegh Roushenas, Maryam Nikzad*, Ali Asghar Ghoreyshi, Mohsen Ghorbani

Faculty of Chemical Engineering, Babol Noshirvani University of Technology, Babol, Iran.

Received: 2021-09-21 Accepted: 2021-11-26 Published: 2022-02-01

ABSTRACT

In this study, pectin/γ-Fe_2O_3/gl nanocomposite was synthesized using a single-step chemical precipitation method and used as an eco-friendly adsorbent to remove Cd^{2+} and Pb^{2+} from aqueous solution. The nanocomposite was characterized by FE-SEM, EDX, FTIR, XRD, VSM, and TEM analyses. The effect of various parameters such as solution pH (2 to 5), contact time (0 to 60 min), initial ion concentration (10 to 200 mg. L^{-1}), and adsorbent dosage (0.1 to 0.4 g.L^{-1}) on the removal efficiency was investigated. The maximum adsorption capacity of Cd (II) in the conditions (pH: 5, dose of adsorbent: 0.2 g.L^{-1}, and contact time:40 min, initial concentration: 50 mg.L^{-1}) and Pb (II) in the conditions (pH: 4.5, dose of adsorbent: 0.1g.L^{-1}, and contact time:30min, initial concentration: 50 mg.L^{-1}) was 470 and 325 mg. g^{-1}, respectively. The adsorption kinetics was studied using several kinetic models including Langmuir isotherm, Freundlich isotherm, Sips isotherm, and Temkin isotherm. Results indicated that the adsorption mechanism could be well represented by the pseudo-second-order model. The equilibrium data of Cd (II) and Pb (II) adsorption were reasonably described by the Sips and Langmuir isothermal models. The positive value of delta H and negative values of delta G exhibit the endothermic and spontaneous nature of the adsorption process.

Keywords: *Pectin/γ-Fe_2O_3/gl nanocomposite, adsorption isotherms, heavy metals, magnetic adsorbent*

How to cite this article

Roushenas S., Nikzad M., Ghoreyshi A.A., Ghorbani M. Magnetic pectin nanocomposite for efficient adsorption of heavy metals from aqueous solution. J. Water Environ. Nanotechnol., 2022; 7(1): 69-88.

DOI: 10.22090/jwent.2022.01.006

INTRODUCTION

With the rapid expansion of industrialization, the extensive use of metals for various applications has also increased. Industrial activities such as refinery, dyeing, electroplating, printing, mining, and tanning generate a huge amount of wastewater containing heavy metals and other tenacious contaminants [1, 2]. Particularly, heavy metals such as Pb(II) and Cd(II) have become one of the major environmental problems universally because of their nonbiodegradable trait, aggregation, and toxicity even at trace levels [3]. The discharge of heavy metals into the aquatic ecosystems has been known as the cause of various health difficulties in humans and other living organisms [4]. Lead is highly toxic and can cause various health problems such as mental disorders, decreased hemoglobin production, brain damage, and associated retardation. It also affects vital parts of the body, such as the reproductive system, the nervous system, and is associated with problems with high blood pressure and anemia[5]. Cadmium (Cd) is a carcinogen in humans, which affects the lungs, kidneys, liver, and reproductive organs [6]. The US Environmental Protection Agency (EPA) for drinking water has determined the allowable amount of lead and cadmium to be less than 0.015 and 0.005 mg.L^{-1}, respectively [7]. To address this problem, numerous treatment technologies, such as chemical oxidation, membrane separation, ion exchange, precipitation, and adsorption have been developed [8]. Most of these techniques require high operational energy and related

* Corresponding Author Email: *m.nikzad@nit.ac.ir*

This work is licensed under the Creative Commons Attribution 4.0 International License.
To view a copy of this license, visit http://creativecommons.org/licenses/by/4.0/.

cost; Moreover, they also bring environmental aftereffects linked to energy utilization [9]. Among these available techniques, adsorption is the most promising method, because of its high yield, low cost, convenience, and easy regeneration of the adsorbent [10, 11].

In recent years, various studies have been conducted to develop adsorbents from environmentally friendly materials[12-16]. Adsorbents of agricultural origin have polymeric groups like lignin, cellulose, hemicellulose, proteins, and pectin as active centers for metal uptake [17]. Pectin is a complex acidic polysaccharide in the middle lamella and the cell wall of higher plant tissues, with unparalleled attributes such as non-toxicity, biodegradability, and having hydroxyl and carboxyl functional groups for chelation of metal ions. [18-20]. Various fruit wastes such as pomelo peel, banana peel, nutmeg rind, passion fruit rind, and citrus peel are rich sources of pectin [19, 20]. Although pectin can be extracted from these sources at a low cost, it can hardly be used directly as an adsorbent. The main deficiencies of the extracted pectin as an adsorbent for the removal of heavy metal and dye are its low stability, difficulty in separation from aqueous solution, and dissolution in acidic media [21]. To address these deficiencies and to obtain a high adsorption performance, pectin has been modified, before being used directly for adsorption. Wang et al. used (pectin / activated carbon microspheres) as adsorbents, prepared by a simple gel method without chemical bonding to adsorb Pb^{2+} ions [22]. Badalamoole et al. Used pectin nanocomposite as an adsorbent to remove dyes and divalent metal ions from aqueous solutions.The maximum adsorption capacity was 1950 $mg.g^{-1}$ for CV, 111 $mg.g^{-1}$ for Cu^{2+} and 130 $mg.g^{-1}$ for Pb^{2+}[23].

There is still very limited information about the adsorption capacity of pectin after chemical modifications. Typical techniques such as centrifugation and filtration for the separation of the adsorbent from the liquid medium result in adsorbent loss and emancipation of adsorbent in water [3]. Using a magnetic field to separate the solid phase from the liquid is an effective method with high separation efficiency without the need for filtration and centrifugation. In this research, a new nanocomposite based on pectin-coated maghemite nanoparticles was synthesized and used to remove hazardous metals from an aqueous solution. This nanocomposite possesses both the properties of pectin as a good adsorbent as well as iron oxide as a good magnetic material. The co-precipitation method followed by the encapsulation of the maghemite with pectin and cross-linking with calcium ions was employed to produce a pectin-coated iron oxide magnetic nanostructure. Consequently, modification of pectin/g-Fe_2O_3 by chelation groups of N-H was carried out. The synthesized adsorbent was characterized by Fourier transform infrared (FTIR) spectroscopy, X-ray diffraction (XRD), Scanning electron microscopy (FESEM), transmission electron microscopy (TEM), and vibration sample magnetometer (VSM) analyses. The adsorption demeanor of the modified pectin–iron oxide magnetic adsorbent was studied to remove Pb (II) and Cd (II). The effect of various parameters such as pH, initial concentration of Pb(II) and Cd (II) ions, contact time, adsorbent dosage, and temperature was studied through batch adsorption experiments. Also, kinetic and thermodynamic studies were carried out to determine the mechanism which governs the adsorption process. Adsorption isotherms were also used to interpret the adsorption behavior of the metal ions on the pectin/g-Fe_2O_3 nanocomposite.

MATERIALS AND METHODS

Chemicals

Mature sour oranges (*Citrus aurantium*) were collected from a local market in Amol, Mazandaran, Iran. Iron(II) chloride tetrahydrate ($FeCl_2.4H_2O$), iron(III) chloride)$FeCl_3$(, hydrochloric acid (HCl), ammonium hydroxide (25%)(NH_4OH), lead(II) nitrate ($Pb(NO_3)_2$), cadmium(II) nitrate ($Cd(NO_3)_2$), anhydrous calcium chloride ($CaCl_2$) and sodium hydroxide (NaOH) were purchased from Merck, Germany, and all the solutions were prepared using distilled water. All chemicals were analytical grade and used directly without further purification. Stock solutions of 500 $mg.L^{-1}$ Pb(II) and Cd(II) were prepared from the $Pb(NO_3)_2$ and $Cd(NO_3)_2.4H_2O$ (Merck) precursors in the distilled water. These solutions were consequently diluted to obtain the required concentration.

Preparation of sour orange residue

At first, all sour oranges were washed to remove contaminants with hot water (near boiling point). The skin of the oranges was carefully taken so that the albedo (the white spongy layer attached to the colorful skin) was not taken. The oranges were then squeezed to separate the juice. The residues were

CC BY

then crushed using a crushing machine. To remove foreign materials, they were boiled in 20% ethanol for 20 min while stirred at 500 rpm and then filtered. Eventually, the filtered solid residues were dried in an oven at 80 °C. The dried residues were sealed off and stored at 25 °C for later use.

Pectin extraction

For pectin extraction, 20 g of dried albedo powder was added to a container containing 500 ml (solid/liquid ratio of 1:25) of distilled water. In the next step, by adding hydrochloric acid (2 M), the pH of the solution was adjusted to 2. Then the mixture was stirred on a magnetic stirrer at 400 rpm and 80 °C for 90 min. After that, the mixture was filtered to separate the solids. After cooling, the filtrate was mixed with an equal volume of ethanol (99%) for precipitation. The samples were then centrifuged at 6000 rpm for 20 min to separate the sediment from the alcohol and finally, the precipitate was dried in an oven at 45 °C for 24 h[18].

Preparation of g-Fe_2O_3 magnetic nanoparticle

The g-Fe_2O_3 nanoparticles were prepared via a one-step chemical precipitation method. Briefly, 2 ml of HCl (2M) and 20 ml of distilled water were added to 5.33 g $FeCl_2.4H_2O$ under magnetic stirring to dissolve completely. A specific amount of 6.22 g $FeCl_2$ was dissolved in 38 ml of distilled water under stirring conditions for 30 min and added to the previous solution. Later, 600 ml of 2 M ammonium hydroxide solution was added dropwise to the solution in an ultrasonic bath at room temperature, which immediately brown precipitate appeared. Then, the precipitate was washed several times with ethanol and distilled water to remove the residual reagents. After separation with a magnet, the resultant product was dried under vacuum at 40 °C for 24 h.

Preparation of pectin/g-Fe_2O_3 nanocomposite

Pectin/g-Fe_2O_3 nanocomposite was fabricated by chemical oxidation polymerization. In this process, 1 g of pectin was dissolved in 100 ml distilled water (1.0% w/v) and stirred continuously for 24 h. Afterward, 0.2 g of g-Fe_2O_3 nanoparticles were dispersed in a water distillation using an ultrasonic bath and added to the pectin solution. Then, 50 ml of $CaCl_2$ solution as a cross-linking agent was added to the solution dropwise. The resulting solution was then stirred at 500 rpm for 6 h. The magnetic nanocomposite was then separated using a magnet and washed several times with distilled water and finally dried in an oven at 40 °C for 24 h.

Modification of pectin/g-Fe_2O_3 nanocomposite

The main purpose of this modification is to increase adsorption sites and improve adsorption properties. Firstly, 0.1 g of nanocomposite was dispersed in 50 ml of distilled water in an ultrasonic bath. Then, 1 ml glutaraldehyde was added to the solution and stirred at 300 rpm for 30 min. In the next step, 1 ml ethylene amine was added to the solution. To accelerate the reaction, 2 ml of hydrochloric acid was added dropwise to the solution. Then, using a magnet, the modified nanocomposite was separated and washed several times with distilled water. Finally, it was dried at 50 °C for 24 h and used as an adsorbent.

Characterization

The functional groups presented in the pectin and nanocomposite were identified by Fourier–transform infrared spectrophotometry (FTIR, Spectrum Two, USA) in the range of 400–4000 cm^{-1}. The phase and crystallinity were analyzed using powder X-ray diffraction (XRD) analysis obtained by an X-ray diffractometer (X' Pert Pro, Nederland) in the range of 2θ=10–80°. The mean crystallite size of g-Fe_2O_3 nanoparticles was quantitatively determined from XRD data by employing Debye-Scherrer's equation:

$$D = \frac{K}{\beta \cos\theta} \quad (1)$$

where D is the average crystallite size, K=0.9 is the shape factor, λ is the X-ray wavelength (in nm), $_{\theta}$ is the Bragg diffraction angle, and β is the full width at half maximum (FWHM) of the intense peak (in radians). The hysteresis curves of bare maghemite, pectin/g-Fe_2O_3, and the modified nanocomposite were obtained using a vibrating sample magnetometer (VSM, Meghnatis Daghigh Daneshpajouh, Iran). Field emission scanning electron microscopy (FESEM) (SIGMA VP-500, Czech Republic) was used to observe the surface morphology of the maghemite nanoparticles and the nanocomposite. Also, energy-dispersive X-ray spectroscopy (SIGMA VP-500, Czech Republic) was used to identify the elements of the nanocomposite. To investigate the structure and measure the particle size of the nanocomposite, a transmission electron microscope (TEM,

Zeiss-EM10C-100 KV, Germany) was used. The concentration of Pb(II) and Cd(II) in the solutions was measured by atomic absorption spectroscopy (Buck Scientific, 210-VGP, USA).

Batch adsorption experiments

The efficiency of the adsorption process depends on different factors. To determine the optimum condition, it was necessary to investigate the influence of these factors on the efficiency of the adsorption process. For this purpose, the one-factor-at-the-time (OFAT) approach was used where one parameter was changed while others were kept constant. In the adsorption experiments, the amount of adsorbent (0.1 to 0.4 g. L^{-1}), the initial concentration of lead and cadmium solutions (10 to 200 mg. L^{-1}), the solution pH (2 to 5), and contact time (0 to 60 min) were varied according to the OFAT approach. A specific amount of the adsorbent was mixed with 20 ml of the metal solution at 25 °C and stirred at 12000 rpm. After reaching the equilibrium, the adsorbents were separated magnetically from the aqueous solution by an external magnet (Nd-Fe-B), then the residual concentration of metal ions was analyzed immediately by atomic absorption spectrometry. The removal percentage (%) and the adsorption capability (q_e) of heavy metal ions were obtained from the following equations [24]:

$$q_e = \frac{(C_0 - C_e)V}{M} \quad (2)$$

$$R(\%) = \frac{(C_0 - C_e)}{C_0} \quad (3)$$

where q_e (mg. g^{-1}) is the amount of ion adsorbed at equilibrium, C_0 (mg. L^{-1}) is the initial concentration of ions, C_e(mg.L^{-1}) is the concentration of ions at equilibrium, V (L) is the solution volume, M (g) stands for the mass of the adsorbent and R represents the removal efficiency.

pH_{PZC} measurement

To measure pH_{PZC} values in sequential order of co-precipitation process after each surface modification, the pH drift method was applied. pH drift is preferred over other conventional methods such as titrations because it is less time-consuming, results can be obtained in a few steps using common laboratory apparatuses which indeed lowers the overall expenditure of the experiment and the results are perfectly in accordance with the ones obtained from other applied methods. According to this method, solutions of 0.01 mol.L^{-1} NaCl in 10 ml test tubes were adjusted to pH values of 2 to 8 ($pH_{initial}$) using 0.1 mol.L^{-1} NaOH and 0.1 mol. L^{-1} HCl. Then, 30 mg of pectin/g-Fe_2O_3/gl were added to test tubes and shaken at 250 rpm at 25 °C. After 48 h the final pH (pH_{final}) of samples were measured using a microprocessor pH meter (Hanna Instruments, Inc.) and plotted against initial pH. The intersection point of the resulting curve with the line passing origin (pH_{final}=$pH_{initial}$) gives pH_{PZC}[25].

RESULTS AND DISCUSSION

Characterization of pectin/g-Fe_2O_3/gl

The FTIR spectra of the extracted pectin, magnetic nanoparticles, and nanocomposite are shown in Fig.1(a). In the spectrum of pectin, the prominent broad peak located between 3200 and 3600 cm^{-1} was assigned to O-H stretching vibrations [20], and the peak at around 2934 cm^{-1} was attributed to C-H of CH, CH_2, and CH_3 groups [26]. The adsorption bands at 1646 and 1452 cm^{-1} were ascribed to the asymmetric and symmetric vibrations of free carboxyl groups (COO^-) [26].

In the spectrum of iron oxide nanoparticles, the characteristic peaks at 445 and 562 cm^{-1} were ascribed to the stretching vibration of Fe-O in maghemite. The peaks at 1637 and 3398 cm^{-1} were attributed to the stretching vibrations and bending hydroxyl functional groups of water molecules [27, 28]. Meanwhile, the existence of these mentioned peaks in the spectrum of the pectin/g-Fe_2O_3 nanocomposite, could confirm the successful coating of pectin over the g-Fe_2O_3 surface. The stretching vibration of N-H was observed at 3400 cm^{-1}, which verified the introduction of amide groups on the surface of the nanocomposite [29].

The XRD patterns of g-Fe_2O_3 and pectin/g-Fe_2O_3/gl are illustrated in Fig.1(b). The characteristic diffraction peaks at 2θ=30.22°, 35.64°, 43.33°, 53.79°, 57.26°, and 62.87° which correspond to the (220), (311), (400), (422), (511) and (440) indices, respectively, were observed for both samples. These diffraction peaks are consistent with the characteristic crystalline spinel structure of Fe_3O_4 in the database (JCPDS 88-0315), revealing that g-Fe_2O_3 nanoparticles were successfully incorporated in the nanocomposite matrix [30]. It also shows that the crystalline structure of the compounds did not change during

CC BY

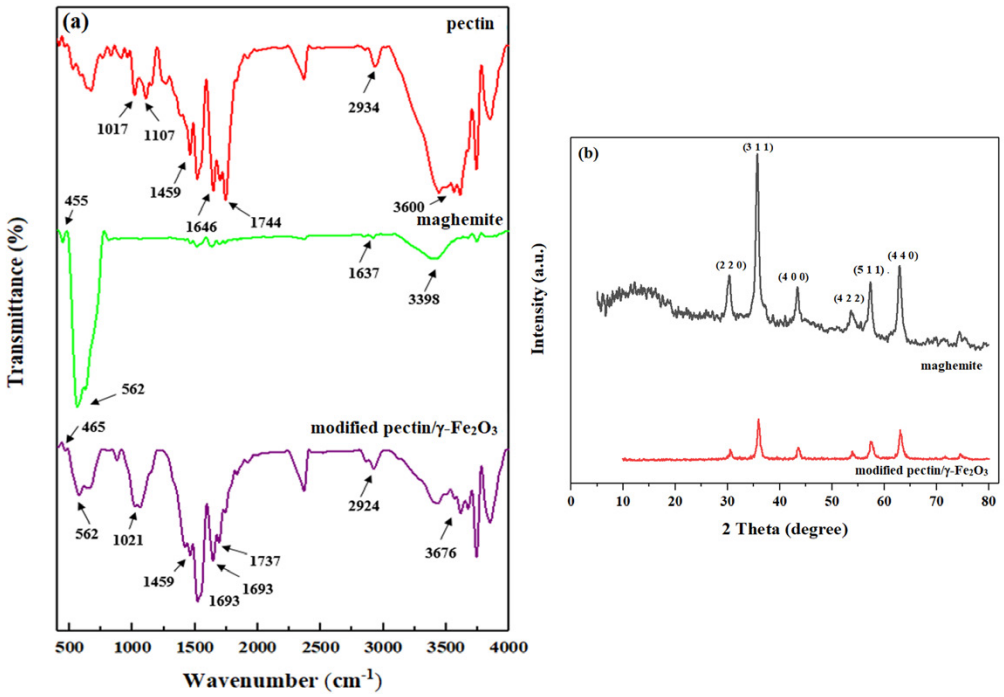

Fig. 1. (a) FTIR spectra of pectin, maghemite nanoparticles, and pectin/γ-Fe_2O_3/gl nanocomposite (b) XRD patterns of maghemite nanoparticles and pectin/γ-Fe_2O_3/gl nanocomposite.

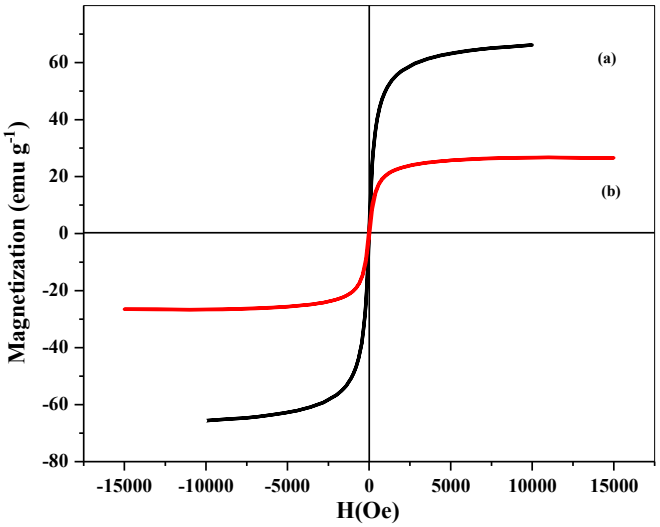

Fig. 2. Magnetization curves of (a) maghemite nanoparticles, and (b) modified pectin/γ-Fe_2O_3/gl nanocomposite.

the synthesis of pectin/g-Fe_2O_3/gl. The reduction of peak intensities in nanocomposites is due to the coating of iron nanoparticles with pectin. The calculated average crystallite size of g-Fe_2O_3 was equal to 14 nm which was consistent with the reported value in the literature [25].

The magnetic property of g-Fe_2O_3 nanoparticles and pectin/g-Fe_2O_3/gl composite was studied using VSM analysis. The results are depicted in Fig. 2. The saturation magnetization magnitudes (M_s) of g-Fe_2O_3 and pectin/g-Fe_2O_3/gl were found to be 66.10 and 26.58 emu. g^{-1}, respectively. The lower saturation magnetization of pectin/g-Fe_2O_3 was attributed to the magnetically inactive pectin [31].

(cc) BY

The residual magnetization and coercivity were zero when the applied magnetic field approached zero. As presented in Fig. 2, the remanence (residue magnetization) and coercive force are close to zero, and the hysteresis loops of g-Fe_2O_3 and pectin/g-Fe_2O_3/gl composite showed the superparamagnetic property. The results indicated that g-Fe_2O_3 was successfully incorporated into the pectin, and the prepared magnetic adsorbent was expected to be separated easily by external magnetic fields [31, 32].

The particle size and surface morphology of the synthesized g-Fe_2O_3 nanoparticles and pectin/g-Fe_2O_3/gl nanocomposites investigated by FESEM analysis is shown in Fig. 3a. Fig. 3(a) displays g-Fe_2O_3 nanoparticles with a diameter in the range of 17 to 30 nm, which were almost spherical and well dispersed. As clearly seen in Fig. 3(a), pectin/g-Fe_2O_3 nanocomposite exhibited a rough surface with granular morphology and the diameter size was in the range of 27 to 45 nm. This image indicates that pectin was successfully coated on the g-Fe_2O_3 nanoparticles.

The EDS spectrum of pectin/g-Fe_2O_3/gl to identify the elements in the nanocomposite is depicted in Fig. 3(b). The existence of pectin and g-Fe_2O_3/gl in the nanocomposite could be confirmed by the peaks of C, O, and Fe. The percentage composition of the elements was found to be in the following order: Fe>O>C. Also, the EDS spectra of the spent adsorbents (after adsorption) revealed the presence of lead and cadmium metals

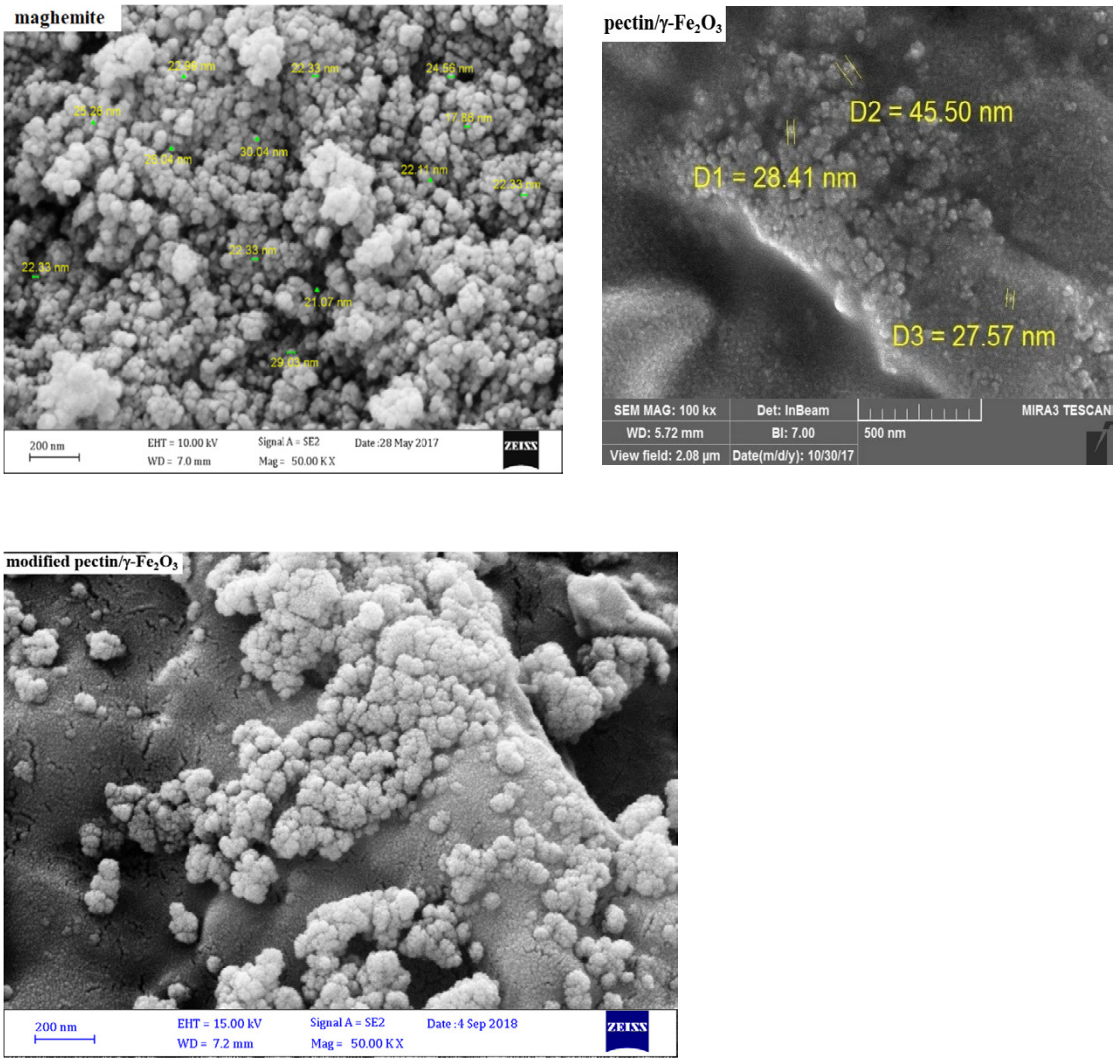

Figure 3 a. The FESEM images of maghemite nanoparticles, pectin/γ-Fe_2O_3 nanocomposite, and pectin/γ-Fe_2O_3/gl nanocomposite

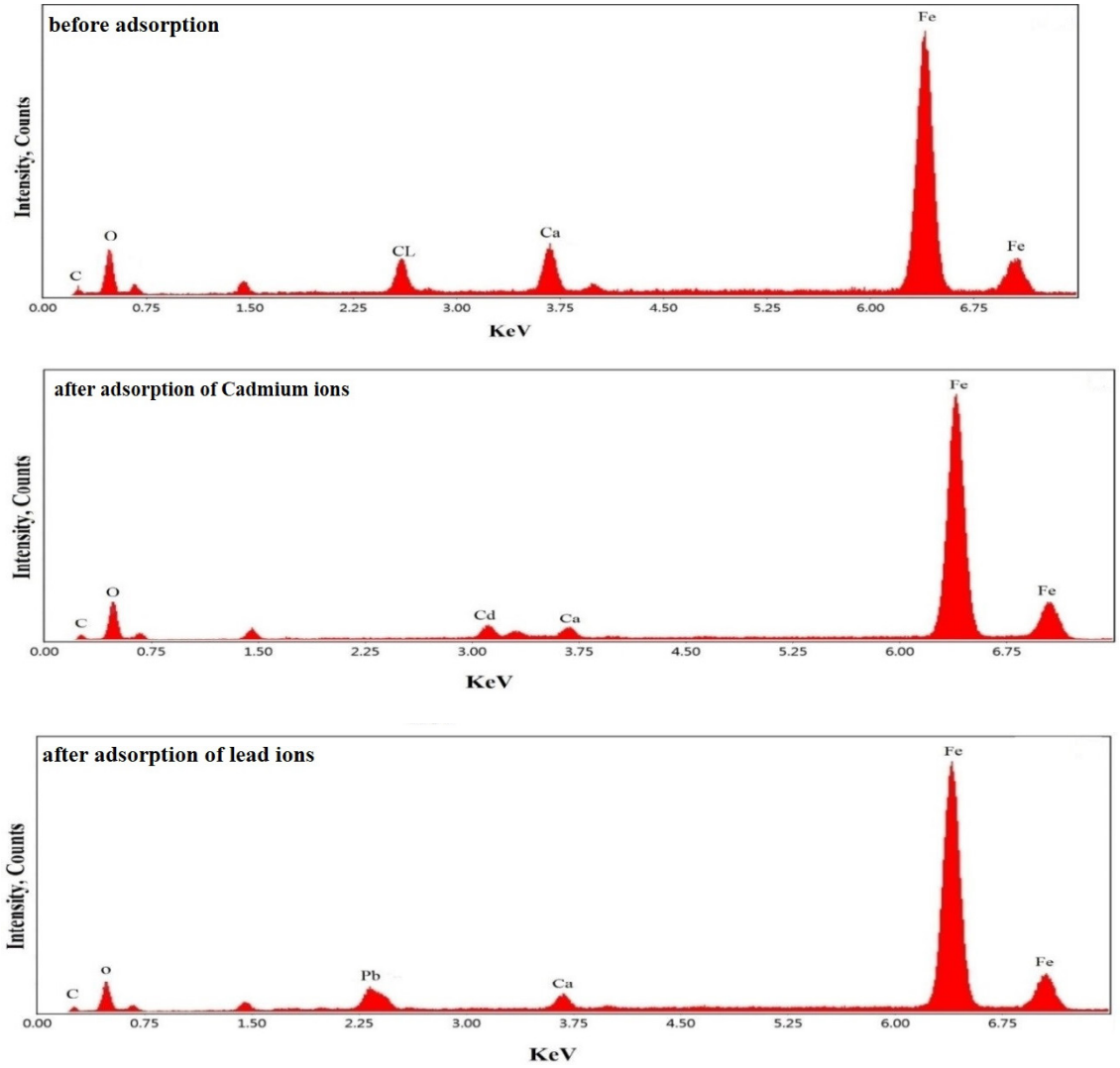

Fig. 3 b. The EDS spectra of adsorbent before adsorption, after adsorption of lead ions, and after adsorption of cadmium ions.

on the adsorbent surface.

Fig 4 shows the TEM micrograph of the pectin/g-Fe_2O_3 nanocomposite. The dark spots correspond to the magnetic core, while the gray contrast indicates the pectin coated on the g-Fe_2O_3 nanoparticles. The images show that the g-Fe_2O_3 nanoparticles were uniformly dispersed inside the pectin matrix. Based on the TEM analysis, it can be observed that the size of pectin/g-Fe_2O_3 nanocomposite is less than 50 nm

Adsorption of lead and cadmium ions

pH_{PZC} values

Fig.5 shows the pH_{final} curves in $pH_{initial}$ terms for the nanocomposite, where the pH_{PZC} values obtained are about 5. For pH values below the zero charge point, a positive pH shift occurred and for values greater than a zero charge point, a negative pH shift occurred. In other words, at pH> pH_{PZC}, protonation of surface functional groups increases the concentration of H^+ ions in the environment and on the other hand increases the concentration of O^- ions on the nanocomposite surface, resulting in a negatively charged nanocomposite surface [25].

Effect of solution pH

The adsorption of metal ions on the adsorbents significantly depends on the solution pH because pH influences the adsorbent surface charge and the

(cc) BY

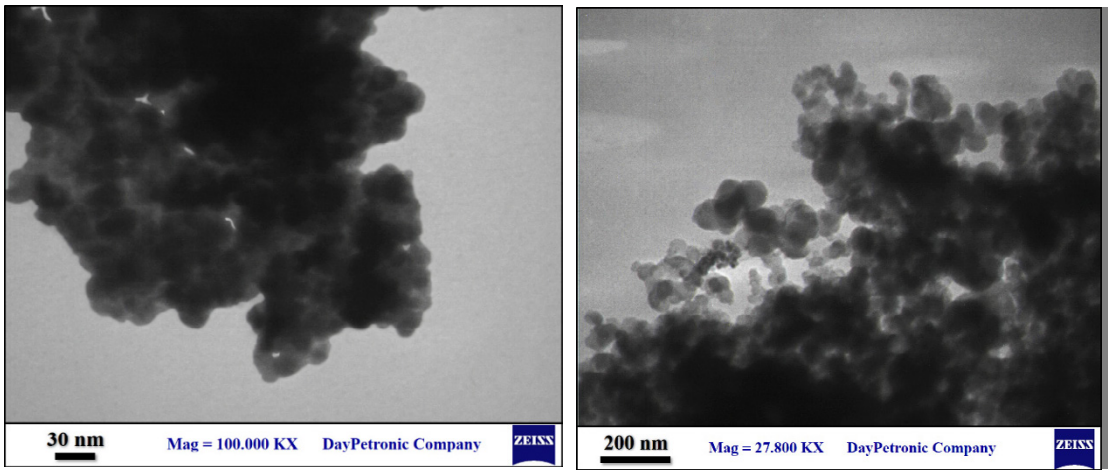

Fig. 4. TEM images of pectin/γ-Fe_2O_3 nanocomposite.

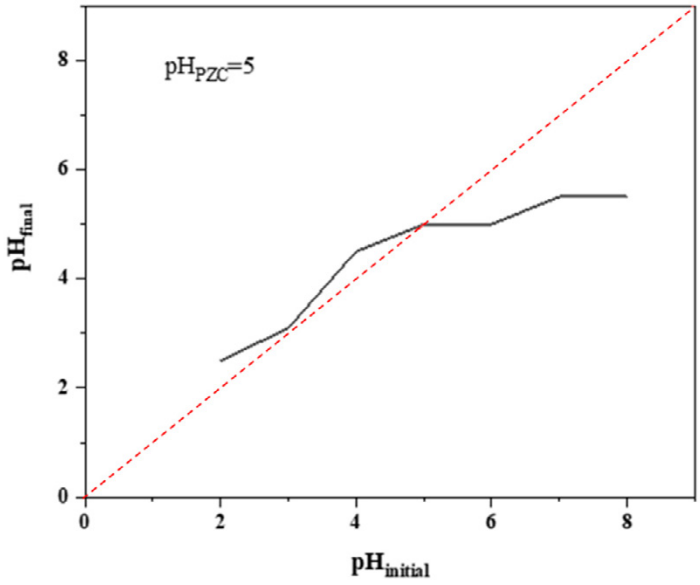

Fig. 5. The pH_{PZC} content of the pectin/γ-Fe_2O_3/gl nanocomposite.

protonation degree and speciation of ions in the solution [3]. The effects of the solution pH on lead and cadmium removal at pH 2-6are shown in Fig. 6 with conditions (initial concentration:100 $mg.L^{-1}$, dose of adsorbent: 0.1$g.L^{-1}$, and contact time: 24h).

As lead ions precipitate at pH>5, hence, the effect of pH on lead removal efficiency was investigated at solution pH<5. As shown in Figure 5, the removal percentage of metal ions is enhanced by an increase in the solution pH. Within the studied pH range, the removal percentage of Cd (II) and Pb (II) increased from 5 to 70%, and 20 to 95%, respectively. This behavior could be attributed to the protonation of the amino and carboxyl groups at low pH, and competitive adsorption of H^+ and H_3O^+ ions with lead and cadmium ions for similar binding sites. In other words, at low pH, the removal efficiency was less owing to repulsion between positive charges of both adsorbent surface and metal ions. At low pH pectin/g-Fe_2O_3/gl remains in fully protonated form and functions as weak chelating sorbent. However, as the operating pH approaches pH_{ZPC}, the surface becomes charge-less and adsorption is triggered due to the existence of strong chelating groups, like carboxylate, hydroxyl, and amines. Obviously, at high pH values, the deprotonation of the surface

CC BY

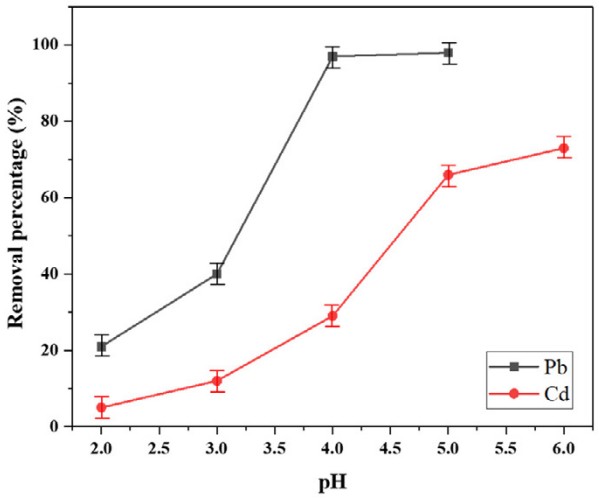

Fig. 6. Effect of pH on the removal percentage (±1.5) of Cd (II) and Pb(II) by pectin/γ-Fe_2O_3/gl (initial concentration:100 mg.L^{-1}, dose of adsorbent: 0.1g.L^{-1}, and contact time: 24h).

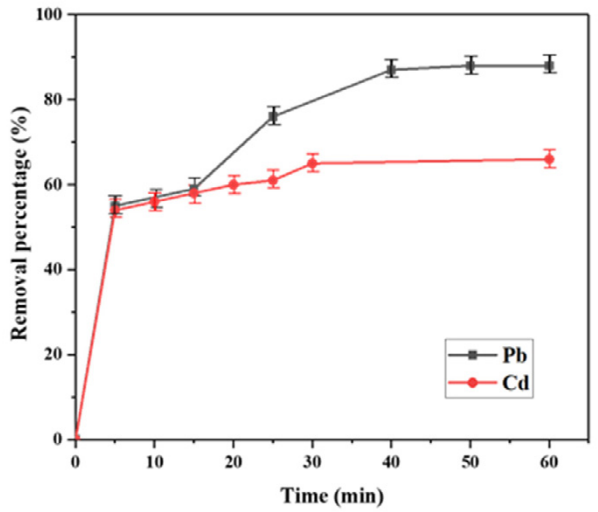

Fig. 7. Effect of contact time on the removal percentage (±0.4) of Cd(II) and Pb(II) by pectin/γ-Fe_2O_3/gl (pH:5, initial concentration: 100 mg.L^{-1}, and dose of adsorbent: 0.1g.L^{-1}).

adsorption sites enhanced the adsorption of heavy metal ions [33, 34]. Based on the obtained results, the most efficient removal of Cd(II) and Pb(II) on the adsorbent occurred at pH 5 and 6, respectively, which were applied for further studies.

Effect of contact time

The removal time of pollutants is an important parameter for the selection of a suitable wastewater treatment method. The effect of contact time on the removal percentage of Cd (II) and Pb (II) (100 mg. L^{-1}) using the pectin/g-Fe_2O_3/gl adsorbent was investigated in the range of 0–60 min at room temperature, while the solution pH was 5 and 6 for the Cd (II) and Pb (II) solutions, respectively. Results regarding the effect of contact time on the removal of cadmium and lead ions are depicted in Fig. 7 with conditions (pH:5, initial concentration: 100 mg.L^{-1}, and dose of adsorbent: 0.1g.L^{-1}). The removal percentage of Cd (II) and Pb (II) increased rapidly within the first 5 min. The removal percentage then gradually reached a plateau after approximately 30 min for cadmium and 40 min for the lead. Afterward, no appreciable changes in terms of separation efficiency were noticed indicating the equilibrium was reached.

CC BY

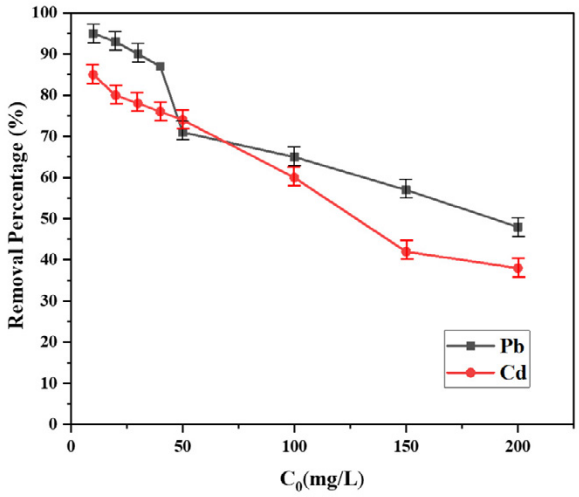

Fig. 8. Effect of Cd(II) and Pb(II) initial concentrations on the removal percentage (±1) by pectin/γ-Fe_2O_3/gl (pH: 5, dose of adsorbent: 0.1g.L^{-1}, and contact time:30-40 min).

Fast uptake of Pb (II) and Cd (II) during the first few minutes of the adsorption was attributed to the availability of a large number of vacant active sites on the adsorbent surface. Cadmium and lead ions occupied most of the available active sites within the first 30 and 40 min of the adsorption, respectively. The reduction of the adsorption rate after these times was due to the decrease of active binding sites on the nanocomposite surface and saturation of the adsorbent. Thus, the optimum contact time was considered as 30 and 40 min for the further adsorption tests for Cd (II) and Pb (II), respectively.

Effect of initial metal ions concentration

The effect of the initial concentration of Cd (II) and Pb (II) on their removal percentage by pectin/g-Fe_2O_3/gl composite was evaluated in the range between 10 to 200 mg. L^{-1}. As illustrated in Fig. 8 with conditions (pH: 5, dose of adsorbent: 0.1g.L^{-1}, and contact time:30-40 min), when the initial concentration of heavy metal ions was increased from 10 to 200 mg. L^{-1}, the removal percentage of Cd (II) and Pb (II) encountered a reduction from 95 to 48%, and 85 to 38%, respectively. This can be explained that at lower initial concentrations, cations could easily access a large number of active sites on the adsorbent surface. While at higher initial concentrations, the access of metal ions to the active sites is limited because the number of binding sites remains the same, and the removal percentage decreases[35].

Effect of adsorbent dosage

The effect of pectin/g-Fe_2O_3/gl nanocomposite dosage on the removal of heavy metal ions was investigated and the results are shown in Fig. 9 with conditions (pH:5, initial concentration: 50 mg.L^{-1}, and contact time: 30-40 min). It was observed that the heavy metal removal efficiency increased up to an optimum dosage of 0.1 and 0.2 g. L^{-1} for Pb (II) and Cd (II), respectively, beyond which the removal percentage did not change remarkably. This result was expected because, for a certain initial concentration of metal ions, increasing the adsorbent dosage provides more active adsorption sites for the adsorbate. On the other hand, by increasing the adsorbent dosage, the number of unsaturated binding sites increases, reducing the adsorption capacity per unit mass of the adsorbent [36].

Adsorption kinetics

In order to investigate the kinetics of Cd (II) and Pb (II) ions adsorption on the pectin/g-Fe_2O_3/gl nanocomposite, two kinetic models, namely pseudo-first-order and pseudo-second-order models, were adopted to fit the experimental data (Fig. 10).

The linearized form of the pseudo-first-order model is expressed:

$$ln(q_e - q_t) = lnq_e - k_1 t \quad (4)$$

The linearized form of the pseudo-second-

CC BY

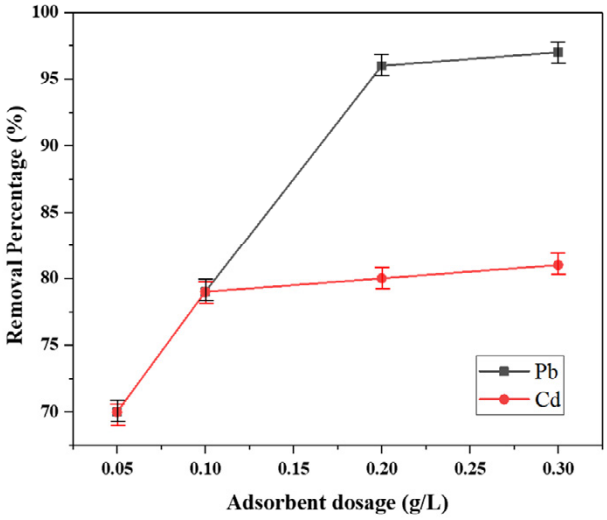

Fig. 9. Effect of adsorbent dosage on the removal percentage (±0.7) of Cd(II) and Pb(II) (pH:5, initial concentration: 50 mg.L^{-1}, and contact time: 30-40 min).

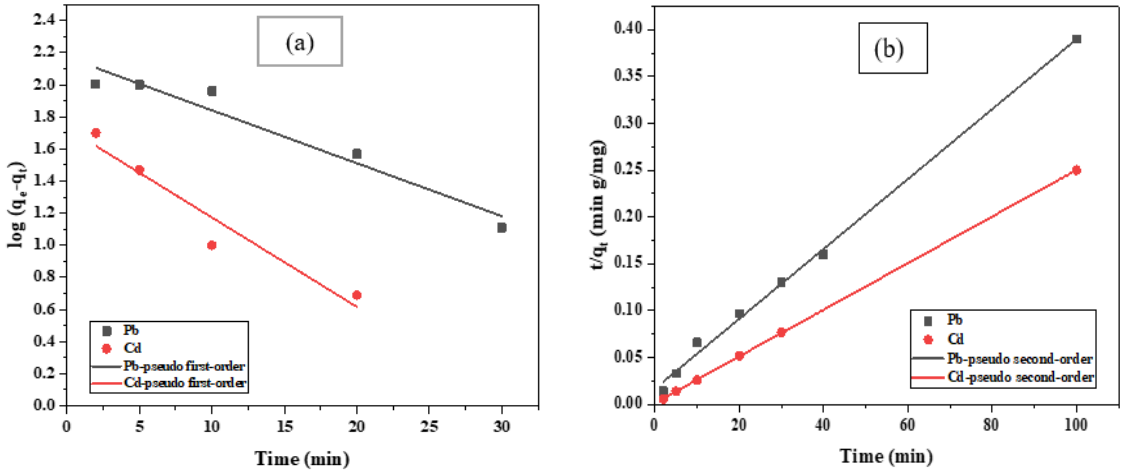

Fig. 10. (a) Pseudo-first-order kinetic model and (b) pseudo second-order kinetic model for Pb(II) and Cd(II) adsorption on pectin/γ-Fe_2O_3/gl nanocomposite.

order model is described as:

$$\frac{t}{q_t} = \frac{1}{k_2 q_e^2} + \frac{1}{q_e} t \qquad (5)$$

where q_e and q_t (mg. g^{-1}) is the amount of adsorbed Cd (II) and Pb (II) ions at equilibrium and contact time t (min), respectively. k_1(min^{-1}) and k_2(g.mg^{-1}.min^{-1}) are the pseudo-first-order and pseudo-second-order rate constants, respectively [37]. The corresponding kinetic parameters and correlation coefficients (R^2) of these models are listed in Table 1. The pseudo-second-order model fitted the experimental data better than the pseudo-first-order model, as illustrated by the higher correlation coefficient. Also, the theoretical values of q_e from the pseudo-second-order kinetic models were much closer to the experimental ones. Similar results have been reported for the adsorption of cadmium and lead ions. According to these results, the Cd(II) and Pb(II) adsorption process was dominated by chemical reactions through sharing or exchanging of electrons [38].

Adsorption isotherms

In order to determine how cadmium and lead ions interact with the pectin/g-Fe_2O_3/gl

(cc) BY

Table 1. Kinetic parameters of Cd(II) and Pb(II) adsorption onto modified pectin/γ-Fe_2O_3.

Heavy metals	C_0 (mg.L^{-1})	$q_{e,exp}$ (mg.g^{1})	Kinetic models					
			pseudo-first order			Pseudo-second-order		
			q_e (mg.g^{-1})	$k_1 \times 10^2$ (1.min^{-1})	R^2	q_e (mg.g^{-1})	$k_2 \times 10^3$ (g.mg^{-1}. min^{-1})	R^2
Pb^{2+}	50	241	133.35	3.0	0.946	273.22	0.8	0.996
Cd^{2+}	50	362	48.64	5.0	0.931	409.83	4.0	0.999

nanocomposite, adsorption isotherms were used. Four of the most frequently applied adsorption isotherms including Langmuir, Freundlich, Sips, and Temkin were considered.

Langmuir isotherm

Langmuir isotherm predicts the formation of a monolayer on the adsorbent and assumes that adsorption occurs at a fixed number of well-defined sites; each active site can retain one ion. All active sites are energetically equipollent, and there is no interaction between the metal ions. This isotherm determines a limiting adsorption capacity; when the monolayer envelopment is achieved, the uptake is no longer influenced remarkably by the adsorbate transport. The maximum absorption capacity is obtained when the surface is coated by a monolayer of the adsorbate. The Langmuir isotherm is given by:

$$q_e = \frac{q_{max} k_l C_e}{1 + k_l C_e} \quad (6)$$

where q_{max} is the maximum adsorption capacity of the adsorbent (mg.g^{-1}) and k_l is the Langmuir constant (L.mg^{-1}).To describe the affinity between the adsorbent and heavy metal ions, a dimensionless factor is expressed using the following equation [39]:

$$R_L = \frac{1}{1 + k_l C_0} \quad (7)$$

where k_l is the Langmuir constant, C_0 is the initial concentration of metal ions (mg. L^{-1}), and R_L indicates the favorability of the isotherm. Values of R_L >1, R_L= 1, 0<R_L< 1 and R_L= 0 show unfavorable, linear, favorable and irreversible adsorption, respectively. In the present case, for both metals, R_L had a value 0< R_L< 1, which indicates a favorable adsorption process.

Freundlich isotherm

The Freundlich isotherm is based on the assumption that the active adsorption sites are dispensed exponentially concerning the heat of adsorption. It also considers that the more potent adsorption active sites are employed first, and the binding strength declines with the increase in site occupation. This model can be used for describing reversible and non-ideal adsorption. This isotherm represents the heterogeneous surface and multilayer adsorption. The Freundlich isotherm model is given by [39]:

$$q_e = k_f C_e^{1/n} \quad (8)$$

where q_e (mg.g^{-1}) is the equilibrium metal uptake capacity, C_e (mg.L^{-1}) is the residual metal ion concentration, 1/n and K_F refer to the intensity of adsorption, and Freundlich constant, respectively. The values of *n* ranging from 2 to 10 demonstrate good adsorption capacity, 1–2 moderate adsorption capacity, and less than one low adsorption capacity. The calculated parameters of Freundlich adsorption models are reported in Tables 2 and 3.

Sips isotherm

The sips model is a combination of the Freundlich and Langmuir isotherms for forecasting heterogeneous adsorption and is accurate for local adsorption without adsorbent-adsorbent interactions. This model indicates that, at low initial concentrations, equilibrium data follow the Freundlich curve, while they follow Langmuir's trend at higher initial concentrations. The Sips isotherm model is expressed as below:

$$q_e = \frac{q_s (k_S C_e)^{1/n_s}}{1 + (k_S C_e)^{1/n_s}} \quad (9)$$

In this equation, q_S (mg.g^{-1}) and k_S (L.mg^{-1}) have the same meanings as q_{max} and k_l in the Langmuir isotherm, whereas $1/n_s$ is a potency introduced from the Freundlich isotherm to demonstrate the heterogeneity of the adsorption sites [33]. For 0<n_s<1, the adsorption phenomenon is

CC BY

Table 2. Isotherm model parameters for Pb(II) adsorption onto modified pectin/γ-Fe_2O_3/gl.

Adsorption isotherms	T (°K)	295	308	318
Langmuir isotherm model	k_L (L.mg^{-1})	0.00305	0.00391	0.00879
	q_{max} (mg.g^{-1})	1408	1216	768
	R_L	0.868	0.836	0.649
	R^2	0.998	0.997	0.997
Freundlich isotherm model	k_F (mg.g^{-1}.(L.mg^{-1})$^{-1/n}$	6.5	8	15
	1/n	0.843	0.812	0.678
	R^2	0.996	0.992	0.981
Sips isotherm model	q_S(mg.g^{-1})	776	576	512
	$1/n_S$	0.875	0.843	0.812
	R^2	0.996	0.992	0.981
Temkin isotherm model	β_T	128	136	136
	K_T	0.097	0.97	0.11
	R^2	0.930	0.937	0.977

Table 3. Isotherm model parameters for Cd(II) adsorption onto pectin/γ-Fe_2O_3/gl

Adsorption isotherms	T (°K)	295	308	318
Langmuir isotherm model	k_L (L.mg^{-1})	0.0029	0.0038	0.0044
	q_{max} (mg.g^{-1})	2176	1920	1856
	R_L	0.873	0.840	0.819
	R^2	0.948	0.964	0.979
Freundlich isotherm model	k_F (mg.g^{-1}.(L.mg^{-1})$^{-1/n}$)	8.5	11	13.5
	1/n	0.875	0.843	0.812
	R^2	0.911	0.931	0.953
Sips isotherm model	q_S(mg.g^{-1})	544	576	672
	$1/n_S$	2.875	2.473	2.06
	R^2	0.999	0.998	0.999
Temkin isotherm model	β_T	272	288	288
	K_T	0.060	0.062	0.070
	R^2	0.994	0.997	0.998

heterogeneous with possible multisite adsorption. Also, for n_s=1, the adsorption phenomenon represents homogeneous active surfaces and the Sips isotherm model tends to the Langmuir model. Finally, for n_s>1, several adsorbate layers are formed on the adsorbent surface [40].

Temkin isotherm

The Temkin isotherm model takes into account the effects of indirect adsorbate/adsorbate interactions on the adsorption process. This model represents how indirect adsorbent-adsorbate interactions affect the adsorption process [41]. The Temkin isotherm equation may be expressed as follows:

$$q_e = \beta_T \, Ln\left(k_T C_e\right) \tag{10}$$

where K_T is the Temkin isotherm constant (L. g^{-1}), and β_T is a constant related to the heat of sorption (kJ.mol^{-1}). The adsorption of heavy metal ions in an aqueous solution is dependent on the temperature. The effects of temperature on the adsorption of Cd (II) and Pb (II) at different initial concentrations are demonstrated in Fig. 11 and 12. These figures indicate that the adsorption capacity enhanced as the temperature increased. The rise of adsorption capacity with an increase in temperature indicates that the adsorption of Cd (II) and Pb (II) ions by pectin/g-Fe_2O_3/gl was an endothermic process. At high temperatures,

(cc) BY

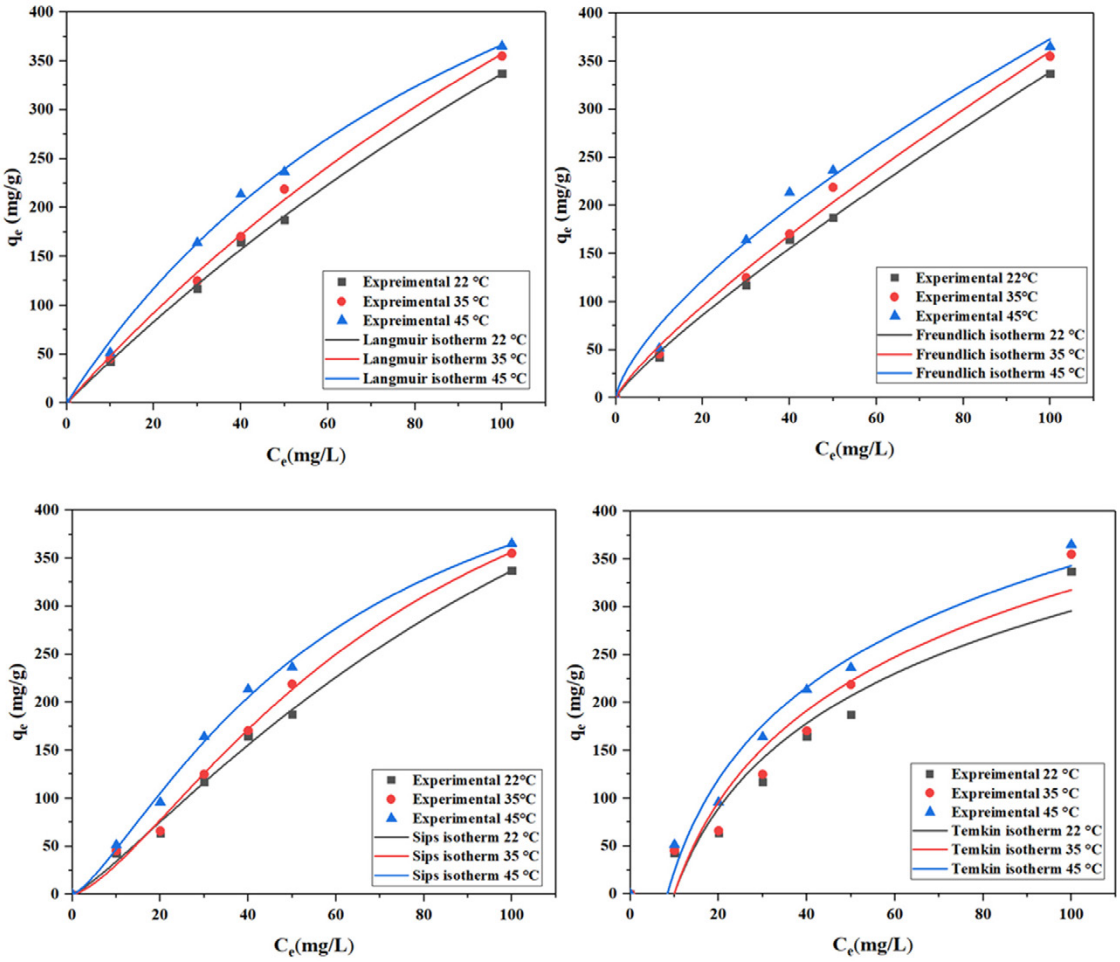

Fig. 11. Langmuir, Freundlich, Sips, and Temkin isotherm models for the adsorption of Pb(II) onto modified pectin/γ-Fe_2O_3/gl nanocomposite at different temperatures.

the rate of heavy metal ions diffusion within the adsorbent network increases, thus the adsorption process accelerates. The initial concentration of heavy metals in the aqueous solution is a vital parameter to provide the driving force for mass transfer between the liquid and solid phases in the adsorption process [42]. To examine this parameter, different initial concentrations were chosen for the batch adsorption of Cd (II) and Pb (II) at three different temperatures; the results are depicted in Fig.11 and 12. The obtained results indicate that the amount of adsorbed metal ions sharply increased when the initial concentration was increased; after that, a gradual enhancement in the adsorption capacity occurred. This could be due to the unoccupied binding sites at lower initial concentrations, but at a higher concentration, they are saturated. The calculated parameters of Langmuir, Freundlich, Temkin, and Sips isotherm models fitted to the collected data at three different temperatures (295, 308, and 318 K) for Cd (II) and Pb (II) are summarized in Tables 2 and 3. The results depict that the Sips model with the highest R^2 value (0.996) is more suitable than the other models to describe the adsorption of cadmium ions satisfactorily. According to the Sips isotherm model, the maximum monolayer Cd (II) adsorption capacity for the nanocomposite was found to be 544 mg. g^{-1}. This value indicates that the developed nanocomposite is a good adsorbent for cadmium removal from aqueous solutions. Also, the fitting of experimental data for lead adsorption onto pectin/g-Fe_2O_3/gl to the four isotherm models indicated that the Langmuir isotherm had the best correlation with the experimental data with an R^2 value of 0.996. It can be concluded that the Langmuir

(cc) BY

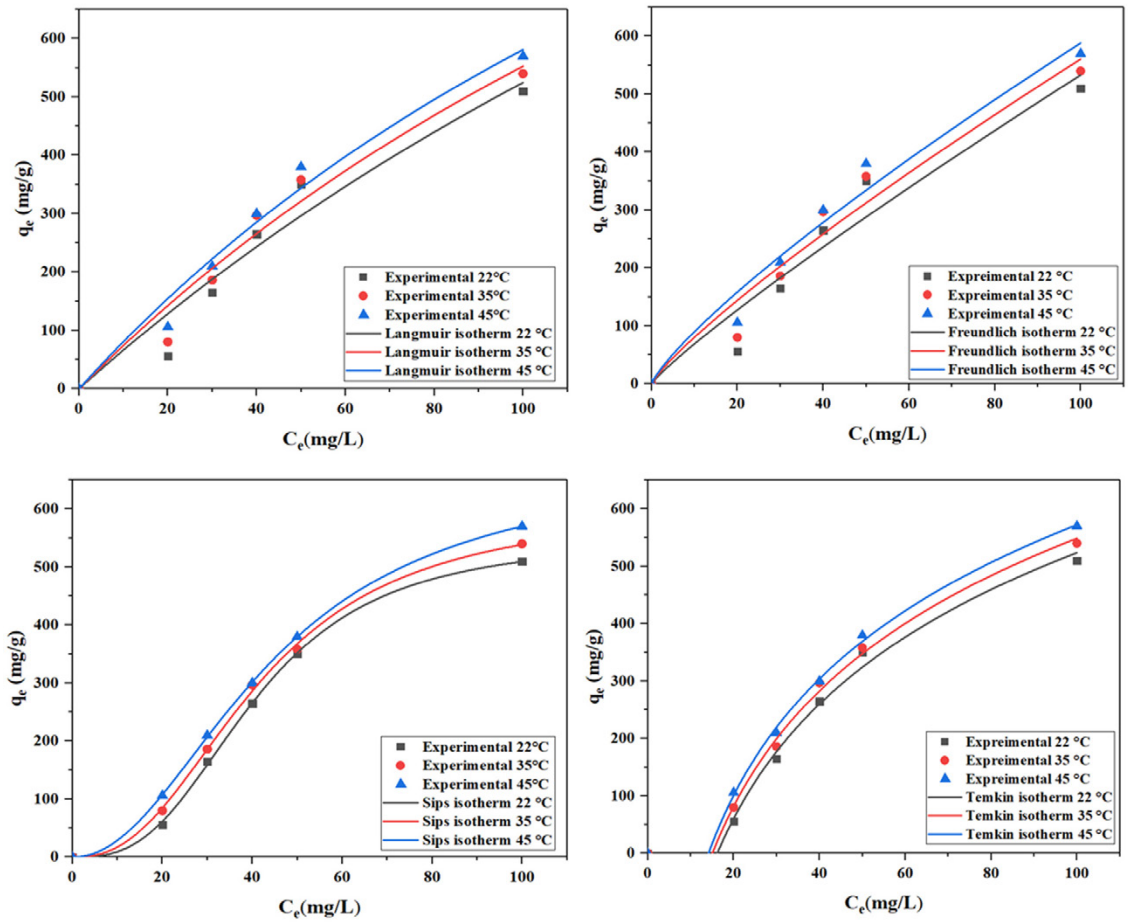

Fig. 12. Langmuir, Freundlich, Sips, and Temkin isotherm models for Cd(II) adsorption onto modified pectin/γ-Fe_2O_3/gl nanocomposite at different temperatures.

isotherm is the best isotherm model to describe the adsorption of Pb (II) ion onto the pectin/g-Fe_2O_3/gl adsorbent. The maximum adsorption capacity of Pb (II) on the pectin/g-Fe_2O_3/gl from the Langmuir model was 1408 mg. g^{-1}.

Adsorption thermodynamics

The thermodynamic of adsorption was studied by calculating the changes in Gibbs free energy (*DG*°), enthalpy (*DH*°), and entropy change (*DS*°). For this purpose, the adsorption of Cd(II) and Pb(II) on the adsorbent was investigated at various temperatures. The values of *DG*°, *DH*°and *DS*° were calculated using the following equations:

$$\Delta G^{\circ} = -RTLnk_L \quad (11)$$

$$K_L = \frac{q_e}{C_e} \quad (12)$$

$$\ln K_L = \frac{\Delta S^0}{R} - \frac{\Delta H^0}{RT} \quad (13)$$

$$\Delta G^{\circ} = \Delta H^{\circ} - T\Delta S^{\circ} \quad (14)$$

where K_L is the distribution coefficient, R is the universal gas constant (8.314 J.mol^{-1}. K^{-1}) and T is the absolute solution temperature (K). The values of *DH*° and *DS*° were obtained from the slope and intercept of Van's Hoff plot of lnK_L versus *1/T*, respectively. The calculated thermodynamic parameters are given in Table 4 and the linear plot of lnK_L versus *1/T* is illustrated in Fig.13.

The negative values of *DG*° for the adsorption of lead and cadmium ions on the magnetic nanocomposite indicate the spontaneous and favorable behavior of the adsorption process. Also,

(cc) BY

Table 4. Thermodynamic parameters for Cd(II) and Pb(II) adsorption by pectin/γ-Fe_2O_3/gl.

Heavy metals	T (**K°**)	**ΔG°** (kJ.mol^{-1})	**ΔS°** (kJ.mol^{-1}.K^{-1})	**ΔH°** (kJ.mol^{-1})
Pb^{2+}	295	-7.10	232	63.85
	303	-9.10		
	313	-11.8		
Cd^{2+}	295	-8.70	96.85	20.366
	303	-9.80		
	313	-10.51		

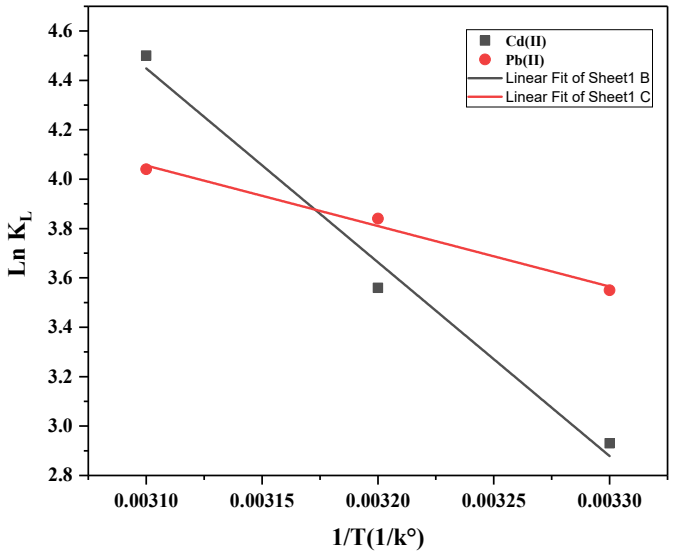

Fig. 13. Van't Hoff plot for Cd (II) and Pb(II) adsorption on pectin/γ-Fe_2O_3/gl nanocomposite.

the positive values of *DH°* show the endothermic adsorption of Cd (II) and Pb (II) ions on pectin/g-Fe_2O_3/gl, where the adsorption capacity grew by increasing the temperature. Due to the fact that the enthalpy for adsorption of lead ions is between 40 and 80 kj.mol^{-1}, the adsorption process is governed by a combination of physical and chemical adsorption, while for cadmium ions the enthalpy is less than 40 kj.mol^{-1}, and the adsorption process is governed by physical adsorption. Also, the positive value of *DS°* demonstrates a system disorder due to an increase in randomness at the solid-liquid interface during the Cd (II) and Pb (II) adsorption process.

Comparison with other works

The pectin/g-Fe_2O_3/gl nanocomposite exhibited magnetic properties along with improved efficiency for the removal of Cd (II) and Pb (II) ions; this could be associated with the higher affinity of the carboxyl, hydroxyl and amino groups to form complexes with heavy metal ions[43]. The maximum theoretical adsorption capacity of pectin/g-Fe_2O_3/gl for lead and cadmium ions was specified by the Langmuir isotherm model that was 1408 and 2176 mg. g^{-1}, respectively. The values of maximum adsorption capacity (q_m) for Cd (II) and Pb (II) ions by other adsorbents are listed in Table 5. As shown in Table 5, the q_m values differ considerably for various sorbents. By comparison, the pectin/g-Fe_2O_3/gl nanocomposite is a promising alternative for the removal of lead (II) and cadmium (II) ions from aqueous solutions.

CONCLUSION

In this study, a new magnetic pectin nanocomposite was synthesized via the precipitation method for the adsorption of cadmium and lead in an aqueous solution. The morphology, structure, and magnetic properties of the synthesized nanocomposite were characterized by various techniques such as FESEM, EDS, TEM,

CC BY

Table 5. Comparison of q_m values for Cd(II) and Pb(II) ions adsorption on different adsorbents.

Metal ions	Adsorbent	Adsorption capacity ($mg.g^{-1}$)	Reference
Cd^{2+}	Graphene oxide modified with 2,20-dipyridylamine	257.201	[44]
	Nano-zerovalent iron particles	769.2	[45]
	Polyacrylic acid modified magnetic mesoporous carbon	406.6	[46]
	Magnetic layered double hydroxide/guar gum bio nanocomposites	258	[47]
	MoS_2/SH-MWCNT	66.6	[48]
	L-cystein modified bentonite-cellulose nanocomposite (cellu/cys-bent)	16.12	[49]
	Purified clays	1005	[50]
	Poly amidoamine dendrimer grafted magnetic graphene oxide nanosheets	435.85	[51]
	Alginate/graphene oxide composite aerogel	183.6	[52]
	Pectin/γ-Fe_2O_3/gl nanocomposite	470	In this study
Pb^{2+}	Fe_3O_4/SiO_2-GO	385	[53]
	Pistachio Shell Carbon (PSC)	7.9	[54]
	L-cystein modified bentonite-cellulose nanocomposite (cellu/cys-bent)	18.52	[49]
	groundnut husk modified with Guar Gum	9.76	[55]
	Luffa acutangula (LAPR)	24	[56]
	MnO_2@Fe_3O_4/ poly(m-phenylenediamine)	438	[57]
	GO-$MnFe_2O_4$	673	[58]
	L-methionine MMT encapsulated guar gum-g-polyacrylonitrile (GPCM) hybrid nanocomposite	125	[59]
	$SrHPO_4/Fe_3O_4$ magnetic nanocomposite	1215.5	[60]
	Mentha piperita carbon (MTC)	18	[61]
	Aminosilane modified-SnO_2/Porous silica nanocomposite	653.62	[38]
	Esterified hydroxyapatite (n-EHAP) nanocrystals	2398.33	[62]
	Polyacrylic acid grafted magnetic chitosan	1476.9	[63]
	Fe@MgO magnetic nanocomposites	368.2	[52]
	Alginate-Au-Mica bio nanocomposite	300	[64]
	Pectin/γ-Fe_2O_3/gl nanocomposite	325	In this study

XRD, and FTIR. The synthesized sorbent revealed a fast kinetic process for cadmium and lead ions. The synthesized adsorbent has a magnetic property that results in easy separation by a magnetic field. The data obtained for cadmium and lead ions adsorbed onto pectin/Fe_2O_3 was best described by the pseudo-second kinetic model. The isothermal studies demonstrated that the adsorption data of Cd(II) and Pb(II) were consistent with Sips and Langmuir isotherm models, respectively. The maximum adsorption capacity of Cd(II) and Pb(II) was 470 and 325 $mg.g^{-1}$, respectively. These values are higher than most of the other adsorbents reported. Also, the thermodynamic study revealed that the adsorption process was spontaneous and endothermic. The results of the present work show that pectin/g-Fe_2O_3/gl nanocomposite has great potential to utilize as a nonhazardous and bio adsorbent for effective adsorption of cadmium and lead ions in aqueous solution.

ACKNOWLEDGMENT

This work was supported by Babol Noshirvani University of Technology (BNUT) through the postgraduate student grant BNUT/944150019/1400.

(cc) BY

CONFLICTS OF INTEREST

There are no conflicts to declare.

REFERENCES

1. Sherlala A, Raman A, Bello M, et al. A review of the applications of organo-functionalized magnetic graphene oxide nanocomposites for heavy metal adsorption. Chemosphere. 2018; 193: 1004-1017.
2. Petrovič A, Simonič M. Removal of heavy metal ions from drinking water by alginate-immobilised Chlorella sorokiniana. International journal of environmental science and technology. 2016; 13: 1761-1780.
3. Alizadeh B, Delnavaz M, Shakeri A. Removal of Cd (II) and phenol using novel cross-linked magnetic EDTA/chitosan/TiO_2 nanocomposite. Carbohydrate polymers. 2018; 181: 675-683.
4. Uddin M K. A review on the adsorption of heavy metals by clay minerals, with special focus on the past decade. Chemical Engineering Journal. 2017; 308: 438-462.
5. Manyangadze M, Chikuruwo N M, Narsaiah T B, et al. Adsorption of lead ions from wastewater using nano silica spheres synthesized on calcium carbonate templates. Heliyon. 2020; 6: e05309.
6. Kavand M, Eslami P, Razeh L. The adsorption of cadmium and lead ions from the synthesis wastewater with the activated carbon: Optimization of the single and binary systems. Journal of Water Process Engineering. 2020; 34: 101151.
7. Karunanayake A G, Todd O A, Crowley M, et al. Lead and cadmium remediation using magnetized and nonmagnetized biochar from Douglas fir. Chemical Engineering Journal. 2018; 331: 480-491.
8. Zia Z, Hartland A, Mucalo M. Use of low-cost biopolymers and biopolymeric composite systems for heavy metal removal from water. International journal of environmental science and technology. 2020.
9. Deng J, Liu Y, Liu S, et al. Competitive adsorption of Pb (II), Cd (II) and Cu (II) onto chitosan-pyromellitic dianhydride modified biochar. Journal of colloid and interface science. 2017; 506: 355-364.
10. Yang G, Tang L, Lei X, et al. Cd (II) removal from aqueous solution by adsorption on α-ketoglutaric acid-modified magnetic chitosan. Applied surface science. 2014; 292: 710-716.
11. Yan J, Lan G, Qiu H, et al. Adsorption of heavy metals and methylene blue from aqueous solution with citric acid modified peach stone. Separation Science and Technology. 2018; 53: 1678-1688.
12. Hasan I, Ahamd R. A facile synthesis of poly (methyl methacrylate) grafted alginate@ Cys-bentonite copolymer hybrid nanocomposite for sequestration of heavy metals. Groundwater for Sustainable Development. 2019; 8: 82-92.
13. Ahmad R, Mirza A. Synthesis of Guar gum/bentonite a novel bionanocomposite: Isotherms, kinetics and thermodynamic studies for the removal of Pb (II) and crystal violet dye. Journal of Molecular Liquids. 2018; 249: 805-814.
14. Ahmad R, Mirza A. Facile one pot green synthesis of Chitosan-Iron oxide (CS-Fe_2O_3) nanocomposite: Removal of Pb (II) and Cd (II) from synthetic and industrial wastewater. Journal of Cleaner Production. 2018; 186: 342-352.
15. Ahmad R, Mirza A. Adsorptive removal of heavy metals and anionic dye from aqueous solution using novel Xanthan gum-Glutathione/Zeolite bionanocomposite. Groundwater for Sustainable Development. 2018; 7: 305-312.
16. Mirza A, Ahmad R. Novel recyclable (Xanthan gum/montmorillonite) bionanocomposite for the removal of Pb (II) from synthetic and industrial wastewater. Environmental Technology and Innovation. 2018; 11: 241-252.
17. Anwar J, Shafique U, Salman M, et al. Removal of Pb (II) and Cd (II) from water by adsorption on peels of banana. Bioresource technology. 2010; 101: 1752-1755.
18. Raji Z, Khodaiyan F, Rezaei K, et al. Extraction optimization and physicochemical properties of pectin from melon peel. International journal of biological macromolecules. 2017; 98: 709-716.
19. Attallah O A, Al-Ghobashy M A, Nebsen M, et al. Removal of cationic and anionic dyes from aqueous solution with magnetite/pectin and magnetite/silica/pectin hybrid nanocomposites: kinetic, isotherm and mechanism analysis. RSC advances. 2016; 6: 11461-11480.
20. Jafari F, Khodaiyan F, Kiani H, et al. Pectin from carrot pomace: Optimization of extraction and physicochemical properties. Carbohydrate polymers. 2017; 157: 1315-1322.
21. Gong J-L, Wang X-Y, Zeng G-M, et al. Copper (II) removal by pectin–iron oxide magnetic nanocomposite adsorbent. Chemical Engineering Journal. 2012; 185: 100-107.
22. Wang R-s, Li Y, Shuai X-x, et al. Pectin/Activated Carbon-Based Porous Microsphere for Pb^{2+} Adsorption: Characterization and Adsorption Behaviour. Polymers. 2021; 13: 2453.
23. Kodoth A K, Badalamoole V. Silver nanoparticle-embedded pectin-based hydrogel for adsorptive removal of dyes and metal ions. Polymer Bulletin. 2020; 77: 541-564.
24. Alqadami A A, Khan M A, Otero M, et al. A magnetic nanocomposite produced from camel bones for an efficient adsorption of toxic metals from water. Journal of Cleaner Production. 2018; 178: 293-304.
25. Gatabi M P, Moghaddam H M, Ghorbani M. Point of zero charge of maghemite decorated multiwalled carbon nanotubes fabricated by chemical precipitation method. Journal of Molecular Liquids. 2016; 216: 117-125.
26. Pasandide B, Khodaiyan F, Mousavi Z E, et al. Optimization of aqueous pectin extraction from Citrus medica peel. Carbohydrate polymers. 2017; 178: 27-33.
27. Nematollahzadeh A, Seraj S, Mirzayi B. Catecholamine coated maghemite nanoparticles for the environmental remediation: Hexavalent chromium ions removal. Chemical Engineering Journal. 2015; 277: 21-29.
28. Kord Mostafapour F, Bazrafshan E, Farzadkia M, et al. Arsenic removal from aqueous solutions by Salvadora persica stem ash. Journal of Chemistry. 2013; 2013.
29. Kulal P, Badalamoole V. Magnetite nanoparticle embedded Pectin-graft-poly (N-hydroxyethylacrylamide) hydrogel: Evaluation as adsorbent for dyes and heavy metal ions from waste water. International journal of biological macromolecules. 2020; 156: 1408-1417.
30. Huang D, Wu J, Wang L, et al. Novel insight into adsorption and co-adsorption of heavy metal ions and an organic pollutant by magnetic graphene nanomaterials in water. Chemical Engineering Journal. 2019; 358: 1399-1409.
31. Okoli C P, Ofomaja A E. Degree of time dependency of kinetic coefficient as a function of adsorbate concentration;

CC BY

new insights from adsorption of tetracycline onto monodispersed starch-stabilized magnetic nanocomposite. Journal of environmental management. 2018; 218: 139-147.
32. Ding Y, Shen S Z, Sun H, et al. Design and construction of polymerized-chitosan coated Fe_3O_4 magnetic nanoparticles and its application for hydrophobic drug delivery. Materials Science and Engineering: C. 2015; 48: 487-498.
33. Fallah TAlooki E, Ghorbani M, Ghoreyshi A A. Investigation of α-iron oxide-coated polymeric nanocomposites capacity for efficient heavy metal removal from aqueous solution. Polymer Engineering and Science. 2015; 55: 2735-2742.
34. Bhunia P, Chatterjee S, Rudra P, et al. Chelating polyacrylonitrile beads for removal of lead and cadmium from wastewater. Separation and Purification Technology. 2018; 193: 202-213.
35. Mittal J, Ahmad R, Mariyam A, et al. Expeditious and enhanced sequestration of heavy metal ions from aqueous environment by papaya peel carbon: a green and low-cost adsorbent. Desalination and Water Treatment. 2021; 210: 365-376.
36. Al-Senani G M, Al-Fawzan F F. Adsorption study of heavy metal ions from aqueous solution by nanoparticle of wild herbs. The Egyptian Journal of Aquatic Research. 2018; 44: 187-194.
37. Lee S-J, Park J H, Ahn Y-T, et al. Comparison of heavy metal adsorption by peat moss and peat moss-derived biochar produced under different carbonization conditions. Water, Air, and Soil Pollution. 2015; 226: 9.
38. Kheshtzar I, Ghorbani M, Gatabi M P, et al. Facile synthesis of smartaminosilane modified-SnO_2/porous silica nanocomposite for high efficiency removal of lead ions and bacterial inactivation. Journal of hazardous materials. 2018; 359: 19-30.
39. Taha A, Shreadah M A, Ahmed A, et al. Multi-component adsorption of Pb (II), Cd (II), and Ni (II) onto Egyptian Na-activated bentonite; equilibrium, kinetics, thermodynamics, and application for seawater desalination. Journal of Environmental Chemical Engineering. 2016; 4: 1166-1180.
40. Vieira R M, Vilela P B, Becegato V A, et al. Chitosan-based hydrogel and chitosan/acid-activated montmorillonite composite hydrogel for the adsorption and removal of Pb^{2+} and Ni^{2+} ions accommodated in aqueous solutions. Journal of Environmental Chemical Engineering. 2018; 6: 2713-2723.
41. Długosz O, Banach M. Kinetic, isotherm and thermodynamic investigations of the adsorption of Ag^{+} and Cu^{2+} on vermiculite. Journal of Molecular Liquids. 2018; 258: 295-309.
42. Shafizadeh F, Taghizadeh M, Hassanpour S. Preparation of a novel magnetic Pd (II) ion-imprinted polymer for the fast and selective adsorption of palladium ions from aqueous solutions. Environmental Science and Pollution Research. 2019; 26: 18493-18508.
43. Motahari S, Nodeh M, Maghsoudi K. Absorption of heavy metals using resorcinol formaldehyde aerogel modified with amine groups. Desalination and Water Treatment. 2016; 57: 16886-16897.
44. Zare-Dorabei R, Ferdowsi S M, Barzin A, et al. Highly efficient simultaneous ultrasonic-assisted adsorption of Pb (II), Cd (II), Ni (II) and Cu (II) ions from aqueous solutions by graphene oxide modified with 2, 2′-dipyridylamine: central composite design optimization. Ultrasonics sonochemistry. 2016; 32: 265-276.
45. Boparai H K, Joseph M, O'Carroll D M. Kinetics and thermodynamics of cadmium ion removal by adsorption onto nano zerovalent iron particles. Journal of hazardous materials. 2011; 186: 458-465.
46. Zeng G, Liu Y, Tang L, et al. Enhancement of Cd (II) adsorption by polyacrylic acid modified magnetic mesoporous carbon. Chemical Engineering Journal. 2015; 259: 153-160.
47. Dinari M, Tabatabaeian R. Ultra-fast and highly efficient removal of cadmium ions by magnetic layered double hydroxide/guargum bionanocomposites. Carbohydrate polymers. 2018; 192: 317-326.
48. Gusain R, Kumar N, Fosso-Kankeu E, et al. Efficient removal of Pb (II) and Cd (II) from industrial mine water by a hierarchical MoS2/SH-MWCNT nanocomposite. ACS omega. 2019; 4: 13922-13935.
49. Ahmad R, Hasan I. L-cystein modified bentonite-cellulose nanocomposite (cellu/cys-bent) for adsorption of Cu^{2+}, Pb^{2+}, and Cd^{2+} ions from aqueous solution. Separation Science and Technology. 2016; 51: 381-394.
50. Mhamdi M, Elaloui E, Trabelsi-Ayadi M. Kinetics of cadmium adsorption by smectite of Oued Tfal (Gafsa Basin). Desalination and Water Treatment. 2014; 52: 4245-4256.
51. Peer F E, Bahramifar N, Younesi H. Removal of Cd (II), Pb (II) and Cu (II) ions from aqueous solution by polyamidoamine dendrimer grafted magnetic graphene oxide nanosheets. Journal of the Taiwan Institute of Chemical Engineers. 2018; 87: 225-240.
52. Pan L, Wang Z, Yang Q, et al. Efficient removal of lead, copper and cadmium ions from water by a porous calcium alginate/graphene oxide composite aerogel. Nanomaterials. 2018; 8: 957.
53. Bao S, Yang W, Wang Y, et al. One-pot synthesis of magnetic graphene oxide composites as an efficient and recoverable adsorbent for Cd (II) and Pb (II) removal from aqueous solution. Journal of hazardous materials. 2020; 381: 120914.
54. Siddiqui S H, Ahmad R. Pistachio Shell Carbon (PSC)–an agricultural adsorbent for the removal of Pb (II) from aqueous solution. Groundwater for Sustainable Development. 2017; 4: 42-48.
55. Ahmad R, Haseeb S. Absorptive removal of Pb^{2+}, Cu^{2+} and Ni^{2+} from the aqueous solution by using groundnut husk modified with Guar Gum (GG): Kinetic and thermodynamic studies. Groundwater for Sustainable Development. 2015; 1: 41-49.
56. Ahmad R, Haseeb S. Kinetic, isotherm and thermodynamic studies for the removal of Pb^{2+} ion by a novel adsorbent Luffa acutangula (LAPR). Desalination and Water Treatment. 2016; 57: 17826-17835.
57. Xiong T, Yuan X, Cao X, et al. Mechanistic insights into heavy metals affinity in magnetic MnO_2@ Fe_3O_4/poly (m-phenylenediamine) core– shell adsorbent. Ecotoxicology and Environmental Safety. 2020; 192: 110326.
58. Kumar S, Nair R R, Pillai P B, et al. Graphene oxide–MnFe2O4 magnetic nanohybrids for efficient removal of lead and arsenic from water. ACS applied materials and interfaces. 2014; 6: 17426-17436.
59. Ahmad R, Hasan I. L-methionine montmorillonite encapsulated guar gum-g-polyacrylonitrile copolymer hybrid nanocomposite for removal of heavy metals. Groundwater for Sustainable Development. 2017; 5: 75-84.

(cc) BY

60. Lu Z, Tan R, Chu W, et al. Synthesis of SrHPO4/Fe3O4 magnetic nanocomposite and its application on Pb2+ removal from aqueous solutions. Microchemical Journal. 2018; 142: 152-158.
61. Ahmad R, Haseeb S. Adsorption of Pb (II) on Mentha piperita carbon (MTC) in single and quaternary systems. Arabian Journal of Chemistry. 2017; 10: S412-S421.
62. Wang M, Zhang K, Wu M, et al. Unexpectedly high adsorption capacity of esterified hydroxyapatite for heavy metal removal. Langmuir. 2019; 35: 16111-16119.
63. Ge L, Wang W, Peng Z, et al. Facile fabrication of Fe@ MgO magnetic nanocomposites for efficient removal of heavy metal ion and dye from water. Powder Technology. 2018; 326: 393-401.
64. Ahmad R, Mirza A. Adsorption of Pb (II) and Cu (II) by Alginate-Au-Mica bionanocomposite: kinetic, isotherm and thermodynamic studies. Process Safety and Environmental Protection. 2017; 109: 1-10.

CC BY